JACS
JOURNAL OF THE AMERICAN CHEMICAL SOCIETY
Communication
pubs.acs.org/JACS

Solid-State Characterization and Photoinduced Intramolecular Electron Transfer in a Nanoconfined Octacationic Homo[2]Catenane

Jonathan C. Barnes,[†,⊥] Marco Frasconi,[†] Ryan M. Young,[†,‡] Nezar H. Khdary,[∥] Wei-Guang Liu,[§] Scott M. Dyar,[†] Paul R. McGonigal,[†] Ian C. Gibbs-Hall,[†] Christian S. Diercks,[†] Amy A. Sarjeant,[†] Charlotte L. Stern,[†] William A. Goddard, III,[§] Michael R. Wasielewski,[†,‡] and J. Fraser Stoddart*[,†]

[†]Department of Chemistry and [‡]Argonne-Northwestern Solar Energy Research (ANSER) Center, Northwestern University, 2145 Sheridan Road, Evanston, Illinois 60208, United States

[§]Materials and Process Simulation Center, California Institute of Technology, 1200 East California Boulevard, Pasadena, California 91125, United States

[∥]National Center for Nano Technology Research, King Abdulaziz City for Science and Technology (KACST) P.O. Box 6086, Riyadh 11442, Kingdom of Saudi Arabia

Supporting Information

ABSTRACT: An octacationic homo[2]catenane comprised of two mechanically interlocked cyclobis(paraquat-*p*-phenylene) rings has been obtained from the oxidation of the septacationic monoradical with nitrosonium hexafluoroantimonate. The nanoconfinement of normally repulsive bipyridinium units results in the enforced π-overlap of eight positively charged pyridinium rings in a volume of <1.25 nm^3. In the solid state, the torsional angles around the C−C bonds between the four pairs of pyridinium rings range between 16 and 30°, while the π−π stacking distances between the bipyridinium units are extended for the inside pair and contracted for the pairs on the outside—a consequence of Coulombic repulsion between the inner bipyridinium subunits. In solution, irradiation of the [2]catenane at 275 nm results in electron transfer from one of the paraphenylene rings to the inner bipyridinium dimer, leading to the generation of a temporary mixed-valence state within the rigid and robust homo[2]catenane.

Viologens,[1] technically referred to as *N*,*N*′-disubstituted-4,4′-bipyridiniums, were first synthesized in the late 19th century by Weidel and Russo.[2] Five decades after their isolation, Michaelis[3] described their semiquinoidal character, namely, their ability to undergo two sequential and reversible one-electron reductions. This observation paved the way for Kosower's[4] and Hünig's[5] research into the radical−radical pairing interactions between two radical cationic methyl viologens ($MV^{\bullet+}\cdots MV^{\bullet+}$) in water. More recently, it has been shown by us[6] that this form of radical molecular recognition can be exploited as a means of templating the formation of 1:1 host−guest complexes[7] and mechanically interlocked molecules[8] (MIMs), such as rotaxanes[9] and catenanes.[10] The introduction of the mechanical bond[8c] into these radical viologen-based MIMs creates a constrained environment in which it is possible for the radical interactions and mixed-valence states to live on indefinitely under an inert atmosphere. Under ambient conditions, however, viologens generally oxidize rapidly back to their dicationic states—a transition which results in the individual components of most MIMs experiencing Coulombic repulsion and undergoing translational motion in order to alleviate the charge strain in accordance with Coulomb's law.

Recently, we reported[10b] a viologen-based MIM **HC**·7PF$_6$ comprised (Scheme 1) of two cyclobis(paraquat-*p*-phenylene) (CBPQT)[11] rings, i.e., a homo[2]catenane (HC), that exists as a stable organic radical under ambient conditions. Moreover, as a consequence of the inherent tight mechanical bonding in the HC, four dicationic viologen subunits are forced to interact with one another, setting the stage for electronic delocalization and the existence of mixed-valence states.[12] Although it was demonstrated[10b] previously that **HC**·7PF$_6$ could be oxidized both electrochemically and chemically, through addition of an excess of tris(4-bromophenyl)ammoniumyl hexachloroantimonate,[13] to generate the octacationic **HC**·8PF$_6$/SbCl$_6$, it was only possible under those conditions to characterize the 8+ oxidation state in solution by ^{1}H NMR spectroscopy on account of stability issues. Subsequently, we have accomplished the chemical oxidation (Scheme 1) of **HC**·7PF$_6$ to **HC**·8SbF$_6$ by using nitrosonium hexafluoroantimonate (**NO**·SbF$_6$), a

Scheme 1. Generation of the Octacationic Homo[2]Catenane HC·8SbF$_6$ by Chemical Oxidation of the Septacationic Homo[2]Catenane HC·7PF$_6$

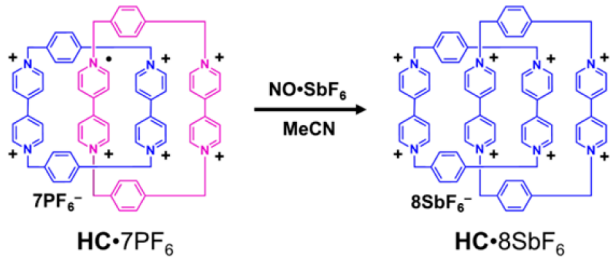

Received: May 21, 2014
Published: July 10, 2014

   dx.doi.org/10.1021/ja505093d | J. Am. Chem. Soc. 2014, 136, 10569−10572

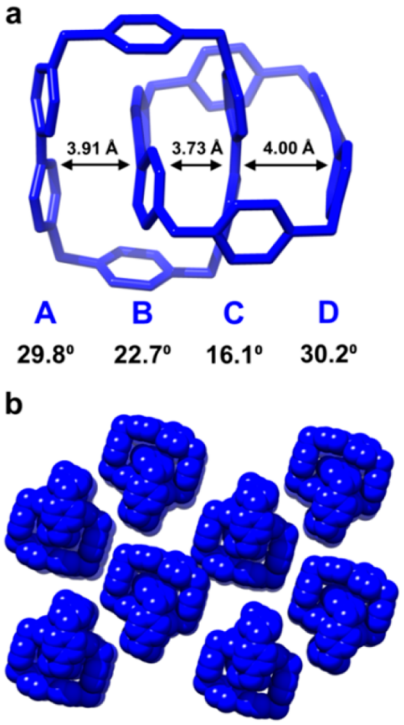

Figure 1. (a) Wireframe representation of the solid-state structure of $\mathbf{HC}^{8+}$ as its SbF_6^- salt showing only C and N atoms. The torsional angles for each viologen unit are displayed directly beneath the corresponding subunit. (b) Space-filling representation of the homo[2]catenane superstructure. All counterions are omitted for the sake of clarity; see the SI for representations of where SbF_6^- counterions are displayed.

strong chemical oxidant, which is converted to a gas (i.e., NO) upon receipt of an electron from **HC**·$7PF_6$. By employing an excess of **NO**·SbF_6 to oxidize **HC**·$7PF_6$, it was possible to obtain single crystals (Figure 1) of the octacation **HC**·$8SbF_6$ that were suitable for X-ray diffraction. Our ability to generate **HC**·$8SbF_6$, and isolate it either in solution or in the solid state, makes this highly charged tetraviologen-based compound a candidate for artificial photosynthetic charge accumulation[14] and potentially as a radical initiator/scavenger in synthetic photochemistry.[15]

In order to investigate the structural changes that occur upon complete oxidation of **HC**·$7PF_6$, a 3 mM MeCN solution of **HC**·$7PF_6$ was treated with 10 equiv of **NO**·SbF_6 as a solid to ensure oxidation and complete counterion exchange to the SbF_6^- salt. The addition of the oxidant led to an immediate change in the color of the solution from dark purple to pale yellow. Single crystals were grown by employing layer-by-layer diffusion of $i\mathrm{Pr}_2\mathrm{O}$ into the oxidized 3 mM MeCN solution of **HC**·$8SbF_6$ inside a capped 538 Wilmad NMR tube. After ∼1 week of diffusion, single crystals of **HC**·$8SbF_6$ were obtained[16] that were suitable for X-ray diffraction. The solid-state structure (Figure 1a) of $\mathbf{HC}^{8+}$ as its SbF_6^- salt reveals two key geometrical differences in comparison to those obtained[10b] for **HC**·$7PF_6$. First, the interplanar distances between the inner and outer viologen subunits (i.e., A to B and C to D) have contracted by ∼0.29 and 0.20 Å, respectively, compared to those (4.20 Å for both) for **HC**·$7PF_6$. This contraction occurs as a consequence of a 0.13 Å expansion (3.60 Å in **HC**·$7PF_6$ compared to 3.73 Å in **HC**·$8SbF_6$) of the interplanar distance between viologen subunits B and C. This expansion results from the loss of radical delocalization between viologen subunits B and C, an interaction which is replaced by Coulombic repulsion between these two dicationic subunits. The second geometrical difference between **HC**·$7PF_6$ and **HC**·$8SbF_6$ is the increase in the torsional angles of each viologen subunit, listed below each letter in Figure 1a. In **HC**·$7PF_6$, the torsional angles for subunits B and C were reported[10b] to be 1.5° and 0.7°, respectively, whereas in the case of **HC**·$8SbF_6$, the torsional angles have increased by more than an order of magnitude (22.7° and 16.1° for subunits B and C, respectively). This increase in the torsional angles between the pyridinium rings of inner viologen subunits B and C also has an effect on the torsional angles of subunits A and D where each one increases by ∼11° when compared to the outer viologen subunits (both 19°) in **HC**·$7PF_6$. Viologens typically[17] "flatten" when reduced from their dicationic oxidation state (V^{2+}) to the monoradical monocation oxidation state ($V^{\bullet+}$) in order to align the *p* orbitals of each pyridinium ring in an effort to delocalize the unpaired radical electrons across the entire viologen subunit. In the case of **HC**·$8SbF_6$, all of the viologen subunits are dicationic and therefore possess high torsional angles between the pyridinium rings of each subunit. The octacationic nature of **HC**·$8SbF_6$ also plays a role in the intermolecular interactions that occur between each HC in the crystal lattice, as evidenced by the packing arrangement observed (Figure 1b) in the superstructure. Each $\mathbf{HC}^{8+}$ in the lattice interacts with another through slipped π–π stacking of adjacent para-phenylene rings. It is important to note that the placement of each $\mathbf{HC}^{8+}$ in the superstructure occurs in order to reduce as much as possible the number of repulsive viologen–viologen interactions.

An investigation of **HC**·$8SbF_6$ in solution (Figure 2) was carried out by treating **HC**·$7PF_6$ with 10 equiv of **NO**·SbF_6, followed by precipitation of **HC**·$8SbF_6$ as a reddish brown solid upon addition of water. Using the freshly generated[18] **HC**·$8SbF_6$, we have been able to characterize the protons of the inner and outer viologen subunits in the ^{1}H NMR spectrum (Figure 2a,b). Four sets of proton signals (two for each set) are observed in total. The H'_β proton signal corresponding to the

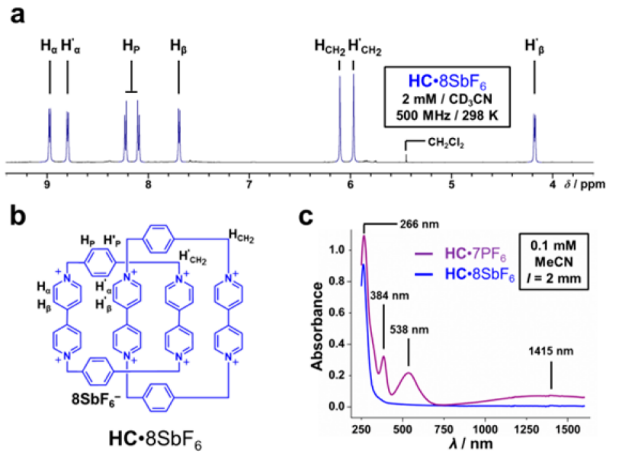

Figure 2. (a) The eight proton resonances observed in the ^{1}H NMR spectrum of **HC**·$8SbF_6$ correspond to (b) four inner protons (H'_α, H'_β, H'_P, and H'_{CH_2}) and four outer protons (H_α, H_β, H_P, and H_{CH_2}). (c) UV–vis absorption spectra for **HC**·$7PF_6$ (purple) and **HC**·$8SbF_6$ (blue) in MeCN. Note the absence of the diagnostic radical bands in the case of **HC**·$8SbF_6$.

dx.doi.org/10.1021/ja505093d | J. Am. Chem. Soc. 2014, 136, 10569–10572

inner viologen subunits (Figure 2b) is shifted upfield to ~4.2 ppm, while the H_β proton signal for the outer viologen subunits resides at ~7.7 ppm. This upfield shift of the H'_β proton occurs as the result of shielding by the paraphenylene ring of the accompanying $CBPQT^{4+}$ component of the HC. See SI for ^{13}C NMR spectrum of **HC**·$8SbF_6$.

UV-vis-NIR optical absorption measurements performed (Figure 2c) on **HC**·$7PF_6$ and **HC**·$8SbF_6$ in MeCN illustrate the loss of the diagnostic radical absorption peak at 538 mm and the broad intervalence band at 1415 nm upon complete oxidation to the octacationic state. The ability to isolate the completely oxidized HC in solution, and the observation that **HC**·$8SbF_6$ absorbs light predominantly between 250 and 300 nm, sets the stage for an investigation into the photophysical properties inherent in this highly charged viologen-based compound.

A 0.125 mM solution of **HC**·$8SbF_6$ in MeCN was prepared by adding 10 equiv of **NO**·SbF_6, followed by precipitation in water and drying under vacuum for several hours, before dissolving the **HC**·$8SbF_6$ sample in dry MeCN. Photoexcitation of the $\pi-\pi^*$ transition of **HC**·$8SbF_6$ at 275 nm (i.e., 4.51 eV) results in an intramolecular electron transfer (IET) process (Figure 3), the kinetics of which can be monitored by femtosecond transient absorption (fsTA) spectroscopy. Figure 3a shows the change in the absorbance of the photoexcited $\mathbf{HC}^{*8+}$ as a function of time (2−7000 ps). A broad absorption band centered at 611 nm emerges in 13 ± 2 ps that is indicative[7b,17a] of a viologen radical cation, followed by charge recombination (Figure 3b), which occurs in 97 ± 4 ps, resulting in charge recombination to regenerate **HC**·$8SbF_6$ in its ground state.

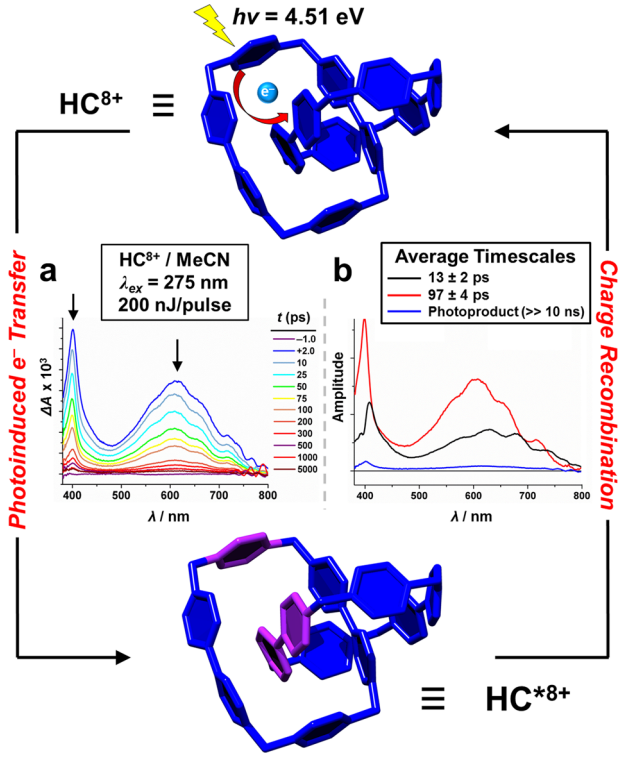

Figure 3. IET occurs upon photoexcitation of $\mathbf{HC}^{8+}$ (top illustration) at 275 nm in MeCN. (a) The diagnostic viologen radical cation absorption band emerges in the visible region at 611 nm. (b) Spectra associated with decay show the short-lived (~100 ps, red trace) mixed-valence state where the purple color in $\mathbf{HC}^{*8+}$ (bottom illustration) symbolizes the charge-separated state, comprised of a radical cation on each subunit. Charge recombination regenerates $\mathbf{HC}^{8+}$.

In order to understand the mechanism of IET, density functional theory was used to calculate[19] the excitation energy of **HC**·$8SbF_6$ in MeCN (4.37 eV) and the gas phase (3.62 eV) as well as to identify the highest occupied molecular orbital (HOMO) and lowest unoccupied molecular orbital (LUMO) of the octacationic oxidation state. Based on these calculations (see the SI for orbital depictions), the HOMO resides on the paraphenylene ring of one of the $CBPQT^{4+}$ ring components of $\mathbf{HC}^{8+}$, while the LUMO resides on the inner tetracationic viologen dimer $(V_2)^{4+}$, designated as subunits B and C in Figure 1a. Upon irradiation of $\mathbf{HC}^{8+}$ (Figure 3, top illustration) at 275 nm, an electron is transferred from an adjacent paraphenylene ring to $(V_2)^{4+}$, a photoinduced process which generates paraphenylene$^{\bullet+}$ (Figure 3, $\mathbf{HC}^{*8+}$, purple ring, bottom illustration) and the mixed-valence dimer $(V_2)^{\bullet3+}$ (Figure 3, $\mathbf{HC}^{*8+}$, purple viologen subunit). This short-lived species quickly undergoes charge recombination to afford $\mathbf{HC}^{8+}$ (Figure 3, top illustration). To confirm that photoexcitation at 275 nm induces electron transfer from the paraphenylene ring, as opposed to being from one of the viologen subunits, control experiments were carried out by photoexciting $\mathbf{MV}^{2+}$, $\mathbf{CBPQT}^{4+}$, and $\mathbf{HC}^{7+}$ separately. See SI for experimental details and spectra. Photoexcitation of $\mathbf{MV}^{2+}$ results in a broad, red-shifted (i.e., ~650 nm) absorption band attributed[20] to the $S_1-S_n^*$ transition, which lives far longer (on the order of ~1 ns) than the photogenerated state $\mathbf{HC}^{*8+}$. Both $\mathbf{CBPQT}^{4+}$ and $\mathbf{HC}^{7+}$ exhibit similar photoexcitation/decay pathways as $\mathbf{HC}^{8+}$ (but lack a photoinduced mixed-valence state) confirming that electron transfer is initiated from the HOMO, namely, the paraphenylene ring. This type of IET mechanism is in line with a recently established[21] pathway observed for the extended bipyridinium-based cyclophane[22] $\mathbf{ExBox}^{4+}$.

In conclusion, we have characterized fully an octacationic homo[2]catenane in the solid state and in solution. We have discovered that the enforced proximity of four dicationic viologen units in a nanoconfined space leads to the emergence of a mixed-valence viologen dimer by way of photoinduced intramolecular electron transfer, wherein the homo[2]catenane functions as both the donor and acceptor when photoexcited at 275 nm. This type of electronic "sink" could potentially function as a multielectron acceptor in artificial photosynthetic systems or as a radical scavenger/initiator in synthetic photochemistry.

■ ASSOCIATED CONTENT

Ⓢ Supporting Information

Synthesis, crystallographic data, and theoretical calculations of **HC**·$8SbF_6$ as well as photoinduced IET data. This material is available free of charge via the Internet at http://pubs.acs.org.

■ AUTHOR INFORMATION

Corresponding Author

stoddart@northwestern.edu

Present Address

[⊥]Department of Chemistry, Massachusetts Institute of Technology, 77 Massachusetts Avenue, Cambridge, Massachusetts 02139, United States

Notes

The authors declare no competing financial interest.

■ ACKNOWLEDGMENTS

This material is based on work supported by the National Science Foundation (NSF) under CHE-1308107. This research is part of the Joint Center of Excellence in Integrated Nano-Systems (JCIN) at King Abdul-Aziz City for Science and Technology (KACST) and Northwestern University (Project 34-947). The authors would like to thank both KACST and Northwestern University (NU) for their continued support of this research. J.C.B. was supported by a National Defense Science and Engineering Graduate Fellowship from the Department of Defense and gratefully acknowledges support from a Ryan Fellowship awarded under the auspices of the NU International Institute of Nanotechnology (IIN). This work was supported by the Chemical Sciences, Geosciences, and Biosciences Division, Office of Basic Energy Sciences, DOE under grant no. DE-FG02-99ER14999 (M.R.W.). Femtosecond spectroscopy (R.M.Y.) was available as part of the ANSER Center, an Energy Frontier Research Center funded by the U.S. Department of Energy, Office of Science, Office of Basic Energy Sciences under award no. DE-SC0001059. W.G.L. and W.A.G. thank NSF (CMMI-1120890 and EFRI-1332411) for financial support and to ONR-DURIP and NSF-CSEM for computing resources.

■ REFERENCES

(1) Monk, P. M. S. *The Viologens: Physicochemical Properties, Synthesis and Applications of the Salts of 4,4′-Bipyridine*; Wiley: New York, 1998.
(2) (a) Weidel, H.; Russo, M. *Monatsh. Chem.* **1882**, *3*, 850−885. (b) Summers, L. A. *The Bipyridinium Herbicides*; American Press: London, 1980.
(3) (a) Michaelis, L.; Hill, E. S. *J. Gen. Physiol.* **1933**, *16*, 859−873. (b) Michaelis, L.; Hill, E. S. *J. Am. Chem. Soc.* **1933**, *55*, 1481−1494. (c) Michaelis, L. *Chem. Rev.* **1935**, *16*, 243−286.
(4) (a) Kosower, E. M.; Cotter, J. L. *J. Am. Chem. Soc.* **1964**, *86*, 5524−5527. (b) Kosower, E. M.; Hajdu, J. *J. Am. Chem. Soc.* **1971**, *93*, 2534−2535.
(5) Hünig, S. *Pure Appl. Chem.* **1967**, *15*, 109−122.
(6) (a) Trabolsi, A.; Khashab, N.; Fahrenbach, A. C.; Friedman, D. C.; Colvin, M. T.; Cotí, K. K.; Benítez, D.; Tkatchouk, E.; Olsen, J.-C.; Belowich, M. E.; Carmielli, R.; Khatib, H. A.; Goddard, W. A., III; Wasielewski, M. R.; Stoddart, J. F. *Nat. Chem.* **2010**, *2*, 42−49. (b) Fahrenbach, A. C.; Zhu, Z.; Cao, D.; Liu, W.-G.; Li, H.; Dey, S. K.; Basu, S.; Trabolsi, A.; Botros, Y. Y.; Goddard, W. A., III; Stoddart, J. F. *J. Am. Chem. Soc.* **2012**, *134*, 16275−16288.
(7) (a) Jeon, W.-S.; Kim, H.-J.; Lee, C.; Kim, K. *Chem. Commun.* **2002**, 1828−1829. (b) Fahrenbach, A. C.; Barnes, J. C.; Lanfranchi, D. A.; Li, H.; Coskun, A.; Gassensmith, J. J.; Liu, Z.; Benítez, D.; Trabolsi, A.; Goddard, W. A., III; Elhabiri, M.; Stoddart, J. F. *J. Am. Chem. Soc.* **2012**, *134*, 3061−3072. (c) Barin, G.; Frasconi, M.; Dyar, S. M.; Iehl, J.; Buyukcakir, O.; Sarjeant, A. A.; Carmieli, R.; Coskun, A.; Wasielewski, M. R.; Stoddart, J. F. *J. Am. Chem. Soc.* **2013**, *135*, 2466−2469.
(8) (a) Schill, G. *Catenanes, Rotaxanes, and Knots*; Academic Press: New York, 1971. (b) *Catenanes, Rotaxanes, and Knots − A JourneyThrough the World of Molecular Topology*; Dietrich-Buchecker, C. O., Sauvage, J.-P., Eds.; Wiley-VCH: Weinheim, 1999. (c) Stoddart, J. F. *Chem. Soc. Rev.* **2009**, *38*, 1802−1820. (d) Forgan, R. S.; Sauvage, J.-P.; Stoddart, J. F. *Chem. Rev.* **2011**, *111*, 5434−5464. (e) Barin, G.; Forgan, R. S.; Stoddart, J. F. *Proc. R. Soc. A* **2012**, *468*, 2849−2880.
(9) Some examples of radical-based rotaxanes: (a) Li, H.; Fahrenbach, A. C.; Dey, S. V.; Basu, S.; Trabolsi, A.; Zhu, Z.; Botros, Y. Y.; Stoddart, J. F. *Angew. Chem., Int. Ed.* **2010**, *49*, 8260−8265. (b) Barnes, J. C.; Fahrenbach, A. C.; Dyar, S. M.; Frasconi, M.; Giesener, M. A.; Zhu, Z.; Liu, Z.; Hartlieb, K. J.; Carmieli, R.; Wasielewski, M. R.; Stoddart, J. F. *Proc. Natl. Acad. Sci. U.S.A.* **2012**, *109*, 11546−11551. (c) Li, H.; Zhu, Z.; Fahrenbach, A. C.; Savoie, B. M.; Ke, C.; Barnes, J. C.; Lei, J.; Zhao, Y.-L.; Lilley, L. M.; Marks, T. J.; Ratner, M. A.; Stoddart, J. F. *J. Am. Chem. Soc.* **2013**, *135*, 456−467.
(10) Some examples of radical-based catenanes: (a) Zhu, Z.; Fahrenbach, A. C.; Li, H.; Barnes, J. C.; Liu, Z.; Dyar, S. M.; Zhang, H.; Lei, J.; Carmieli, R.; Sarjeant, A. A.; Stern, C. L.; Wasielewski, M. R.; Stoddart, J. F. *J. Am. Chem. Soc.* **2012**, *134*, 11709−11720. (b) Barnes, J. C.; Fahrenbach, A. C.; Cao, D.; Dyar, S. M.; Frasconi, M.; Giesener, M. A.; Benítez, D.; Tkatchouk, E.; Chernyashevskyy, O.; Shin, W.-H.; Li, H.; Sampath, S.; Stern, C. L.; Sarjeant, A. A.; Hartlieb, K. J.; Liu, Z.; Carmieli, R.; Botros, Y. Y.; Choi, J. W.; Slawin, A. M. Z.; Ketterson, J. B.; Wasielewski, M. R.; Goddard, W. A., III; Stoddart, J. F. *Science* **2013**, *339*, 429−433.
(11) Odell, B.; Reddington, M. V.; Slawin, A. M. Z.; Spencer, N.; Stoddart, J. F.; Williams, D. J. *Angew. Chem., Int. Ed. Engl.* **1988**, *27*, 1547−1550.
(12) (a) Neta, P.; Richoux, M.-C.; Harriman, A. *J. Chem. Soc., Faraday Trans. 2* **1985**, *81*, 1427−1443. (b) Nelsen, S. F. *Chem.—Eur. J.* **2000**, *6*, 581−588. (c) Sun, D.-L.; Rosokha, S. V.; Lindeman, S. V.; Kochi, J. K. *J. Am. Chem. Soc.* **2003**, *125*, 15950−15963. (d) Sun, D.; Rosokha, S. V.; Kochi, J. K. *J. Am. Chem. Soc.* **2004**, *126*, 1388−1401.
(13) Connelly, N. G.; Geiger, W. E. *Chem. Rev.* **1996**, *96*, 877−910.
(14) (a) Wasielewski, M. R. *Acc. Chem. Res.* **2009**, *42*, 1910−1921. (b) Young, R. M.; Dyar, S. M.; Barnes, J. C.; Juríček, M.; Stoddart, J. F.; Co, D. T.; Wasielewski, M. R. *J. Phys. Chem. A* **2013**, *117*, 12438−12448.
(15) Nicewicz, D. A.; MacMillan, D. W. C. *Science* **2008**, *322*, 77−80.
(16) Crystal Data for $(C_{72}H_{64}N_8F_{48}Sb_8)\cdot 9(C_2H_3N)$ (M = 3296.79): triclinic, space group $P\bar{1}$ (no. 2), a = 16.4947(7), b = 16.7464(7), c = 22.8838(10) Å, α = 86.675(2), β = 78.450(2), γ = 71.512(2)°, V = 5873.4(4) Å^3, Z = 2, T = 100(2) K, ρ_{calc} = 1.864 g/mm^3, μ(CuKα) = 15.493 mm^{-1}. 79636 reflections measured, 21245 unique (R_{int} = 0.0760) which were used in all calculations. R_1 = 0.0886 ($I > 2\sigma(I)$) and wR_2 = 0.2552. CCDC 998871.
(17) (a) Bockman, T. M.; Kochi, J. K. *J. Org. Chem.* **1990**, *55*, 4127−4135. (b) Porter, W. W., III; Vaid, T. P. *J. Org. Chem.* **2005**, *70*, 5028−5035. (c) Fahrenbach, A. C.; Sampath, S.; Late, D. J.; Barnes, J. C.; Kleinman, S. L.; Valley, N.; Hartlieb, K. J.; Liu, Z.; Dyavid, V. P.; Schatz, G. C.; Van Duyne, R. P.; Stoddart, J. F. *ACS Nano* **2012**, *6*, 9964−9971.
(18) Freshly generated **HC**·8SbF$_6$ is stable in the solid state for months at a time. Its stability in solution was monitored by UV-vis-NIR spectroscopy, where the slow reappearance of the radical absorption bands could be observed ∼2 h after dissolution of **HC**·8SbF$_6$ in dry MeCN, possibly the result of a slow electron-transfer process originating from a minor impurity in the solvent. In order to maintain the 8+ oxidation state longer, two drops of 10 mM MeCN solution of **NO**·SbF$_6$ were added to a 3 mM stock solution of **HC**·8SbF$_6$ in 2 mL MeCN. This stock solution was stable for multiple days in a row.
(19) Time-dependent PBE functional with long-range correction was applied to calculate the excitation energy in the gas phase and in MeCN (PCM solvation model, r_{solv} = 2.18, ε = 37.5 and $\varepsilon_{infinity}$ = 1.81), whereas a M06/6-311G**++ basis set was used to generate HOMO/LUMO depictions shown in Figure S6.
(20) Peon, J.; Tan, X.; Hoerner, J. D.; Xia, C.; Luk, Y.-F.; Kohler, B. *J. Phys. Chem. A* **2001**, *105*, 5768−5777.
(21) Dyar, S. M.; Barnes, J. C.; Juríček, M.; Stoddart, J. F.; Co, D. T.; Young, R. M.; Wasielewski, M. R. *Angew. Chem., Int. Ed.* **2014**, *53*, 5371−5375.
(22) (a) Barnes, J. C.; Juríček, M.; Strutt, N. L.; Frasconi, M.; Sampath, S.; Giesener, M. A.; McGrier, P. L.; Bruns, C. J.; Stern, C. L.; Sarjeant, A. A.; Stoddart, J. F. *J. Am. Chem. Soc.* **2013**, *135*, 183−192. (b) Barnes, J. C.; Juríček, M.; Vermeulen, N. A.; Dale, E. J.; Stoddart, J. F. *J. Org. Chem.* **2013**, *78*, 11962−11969. (c) Juríček, M.; Strutt, N. L.; Barnes, J. C.; Butterfield, A. M.; Dale, E. J.; Baldridge, K. K.; Stoddart, J. F.; Siegel, J. S. *Nat. Chem.* **2014**, *6*, 222−228.